J. Fluid Mech. (1985), *vol.* 160, *pp.* 211–234
Printed in Great Britain

On the deformation and drag of a type-A multiple drop at low Reynolds number

By P. O. BRUNN AND T. RODEN
Department of Chemical Engineering and Applied Chemistry, Columbia University, New York, NY 10027

(Received 22 June 1984 and in revised form 6 May 1985)

The dynamics of a perfectly symmetric type-A multiple drop is studied. Up to first order in Reynolds number a force balance predicts the size ratios of the two constituents of such a drop to be unique for each system. Inertial effects are shown (*a*) to be destabilizing and (*b*) to exclude the possibility of obtaining perfectly concentric type-A droplets in a diffusion column. This latter conclusion is strengthened further by the sedimentation results.

1. Introduction

Interest in the motion of particles in a fluid medium has existed for many years. A vast body of literature dealing with bubbles, drops and solid particles has grown up in engineering, applied mathematics and physics. Our understanding of the behaviour of single particles is reviewed by Clift, Grace & Weber (1978).

In multiple emulsions the dispersed drops themselves contain smaller droplets. Depending upon the number and size of internal droplets, the emulsions are classified as type-A, type-B or type-C (Florence & Whitehill 1981). Type-A drops contain one (usually large) internal droplet, type-B drops contain several internal drops, and in type-C drops a vast number of internal droplets are entrapped.

Multiple emulsions are of interest in such diverse fields as the separation of hydrocarbons (Li 1971), blood oxygenation (Li & Asher 1973), treatment of wastewater (Li & Shrier 1972), metal recovery from leaching ores (Martin & Davies 1976), prolongation of drug release (Brodin, Kavaliunas & Frank 1978), and direct-contact heat exchangers (Sideman & Taitel 1964).

Multiple emulsions can be obtained by double emulsification, in which a primary (single) emulsion is reemulsified (Martin & Davies 1976). Depending upon the surfactants used, multiple drops of type A, B or C result (Florence & Whitehill 1981). Multiple droplets of type A can also be obtained in a spray or diffusion column, containing two immiscible liquids, say liquids one and two. Dispersed droplets or bubbles rise through the heavier liquid. A multiple droplet is formed when the single droplet breaks through the previously plane one–two interface (Li & Asher 1973; Mercier *et al.* 1974).

For gas bubbles rising through water and then through mineral oils (as the lower (1) and upper (2) liquid respectively) marked differences in shape, trajectory and rise velocity between the two-phase air–water bubble and normal air bubbles in the same oil have been found (Mercier *et al.* 1974). Since, in that case, the lower liquid (1) has the higher surface tension, all gas bubbles will cross the one–two interphase. According to Selecki & Gradon (1972), no multiple drops should form. Experimentally this is indeed found, although only for bubbles of radius r_1 less than 1.7 mm. At this

critical size the first differences were found, and the terminal rise velocity through the continuous phase two was less than that of the single bubble but larger than for a rigid sphere (of the bubble density) rising through the oil. As a matter of fact, for the most viscous oil used (kinematic viscosity $\nu^{(2)} = 0.55$ cm^2/s) the rigid-sphere limit was almost reached (see figure 3 of Mercier *et al.* 1974). Using the data supplied, we thus see that in this case no difference from the behaviour of single bubbles was found unless the Reynolds number of region i (based on bubble radius) exceeded the values 194.7, 3.5 and 13 in regions one, two and three respectively (three is the inside or bubble region).

In the opposite case, when the lower liquid (1) has the lower surface tension, air bubbles have to exceed a certain critical size in order to break through the interface. According to Selecki and Gradon (1972) the critical radius $r_{i\,cr}$ is given by

$$r_{i\,cr}^2 = \frac{3(\sigma^{(2)} - \sigma^{(1)})}{(\rho^{(1)} + \rho^{(2)})\, g}, \tag{1.1}$$

where $\sigma^{(i)}$ denotes the surface tension of phase i and $\rho^{(i)}$ the mass density. If the lower liquid (1) is Freon 113 ($\rho^{(1)} = 1.58$ g/cm^3, $\sigma^{(1)} = 19$ dyn/cm) and liquid two is a 98.8 % aqueous glycerol solution ($\rho^{(2)} = 1.26$ g/cm^3, $\sigma^{(2)} = 64$ dyn/cm), (1.1) predicts $r_{i\,cr} = 2.20$ mm, quite close to the experimentally determined critical radius of 1.70 mm (Mori *et al.* 1977; see also table 1, system 6B). In addition Selecki & Gradon (1972) conclude that bubbles exceeding that size always have to form multiple drops; and the observation of Mori *et al.* (1977) that the rise velocity is lower than that of a (single) air bubble but larger than that of a rigid sphere seems to substantiate that claim. The lowest Reynolds numbers of Mori *et al.* are 25.6, 1.5×10^{-2} and 0.9 for regions one, two and three respectively.

Both Mercier *et al.* (1972) and Mori *et al.* (1977) observed that the lower liquid encapsulated the air bubble quite non-uniformly, especially for the larger-size bubbles. Studying these configurations may indeed require 'spherical-cap' studies, like the ones introduced by Johnson & Sadhal (1983). To be applicable to the situations at hand, inertial effects have to be incorporated.

Thus multiple drops, produced in a diffusion column, cannot be studied by using a low-Reynolds-number analysis. This contrasts with the double-emulsification technique, where not only perfectly symmetric type-A multiple drops can be obtained (Florence & Whitehall 1981), but in addition the particle Reynolds number is very small in general. It is the purpose of the present study to concentrate on these drops in the low-Reynolds-number range. A complete analysis of multiple drops would not only have to include hydrodynamic factors, but would also have to take account of thermodynamic considerations (including breakdown mechanisms) and the role of surfactants. By concentrating solely on the hydrodynamics, we severely limit the applicability of our results to real systems. Yet, since hydrodynamic considerations do matter, we can discriminate between sensible and useless (future) research. To be more specific, our investigation into perfectly symmetric type-A droplets will be useful only for very specific size ratios (for a given system) in sedimentation.† Studying other size ratios is therefore futile, unless other (non-hydrodynamic) influences are taken into account.

† For all systems studied we do find the perfectly symmetric type-A configuration to be possible in sedimentation. This is astonishing, given the fact that the density ratios used varied considerably: from 8×10^{-4} to 1.29 (inside to shell) and from 0.67 to 1.41 for the shell density relative to the continuous fluid. According to our results, extreme density ratios imply small internal droplets.

In §2 the creeping-motion solution of a spherical drop encapsulating a centrally located spherical drop is studied. In §3 inertial effects are considered and the resulting deformations of each drop (internal and external) are calculated. In §4 we ask whether such a multiple drop can ever attain a terminal state in sedimentation. Comparison with experimental observations will be made throughout the text, and the shortcomings – and strong points – of this analysis will be stated clearly.

This paper constitutes a first attempt towards an understanding of the hydrodynamic factors governing the behaviour of multiple drops. It is hoped that it will stimulate further research in this fascinating and challenging area.

2. Statement of the problem

Consider the axisymmetric streaming flow of an incompressible fluid past a stationary type-A multiple drop. The situation is depicted in figure 1. Denoting by a superscript i the quantity in question appropriate for region i, the steady-state equations of motion and continuity are respectively

$$\left.\begin{aligned} \frac{\partial}{\partial \tilde{\boldsymbol{r}}} \cdot \tilde{\boldsymbol{v}}^{(i)} &= 0, \\ \rho^{(i)}\, \tilde{\boldsymbol{v}}^{(i)} \cdot \frac{\partial}{\partial \tilde{\boldsymbol{r}}}\, \tilde{\boldsymbol{v}}^{(i)} &= -\frac{\partial}{\partial \tilde{\boldsymbol{r}}}\, \tilde{p}^{(i)} + \eta^{(i)}\, \tilde{\nabla}^2 \tilde{\boldsymbol{v}}^{(i)} + \tilde{\boldsymbol{f}}^{(i)}. \end{aligned}\right\} \tag{2.1}$$

We shall assume that the body force per unit volume is conservative,

$$\tilde{\boldsymbol{f}}^{(i)} = -\frac{\partial}{\partial \tilde{\boldsymbol{r}}}\, \tilde{\Phi}^{(i)}, \tag{2.2}$$

which guarantees that a flow-free rest state exists. This being the case, it proves convenient to put

$$\tilde{p}^{(i)} = \hat{p}^{(i)} - \tilde{\Phi}^{(i)}, \tag{2.3}$$

with $\hat{p}^{(i)}$ the hydrodynamic pressure. Note that this split implies

$$\tilde{\boldsymbol{T}}^{(i)} = \Phi^{(i)}\, \boldsymbol{\delta} + \hat{\boldsymbol{T}}^{(i)}, \tag{2.4}$$

with $\hat{\boldsymbol{T}}^{(i)}$ the hydrodynamic part of the stress tensor $\tilde{\boldsymbol{T}}^{(i)}$.

For streaming flow with velocity $\boldsymbol{v}_\infty$ (of magnitude v_∞) in the direction $\hat{\boldsymbol{k}}$ (a unit vector), the faraway boundary conditions are

$$\tilde{\boldsymbol{v}}^{(2)} = \boldsymbol{v}_\infty \quad \text{as } \tilde{r} \to \infty. \tag{2.5}$$

Here $\tilde{r} = |\tilde{\boldsymbol{r}}|$, with $\tilde{\boldsymbol{r}} = (\tilde{r}, \theta, \phi)$ the position vector of some point relative to the centre of the drop. For the type-A multiple drop considered in this study three regions can be defined: the inner dispersed phase three of volume $V_1 = \frac{4}{3}\pi(a\epsilon)^3$, the fluid shell of volume $V_m = \frac{4}{3}\pi a^3(1-\epsilon^3)$ encapsulating this inner region, and the continuous phase, region two, which occupies all space outside region one. Quite clearly, the velocity must be finite at the drop centre, i.e.

$$\tilde{\boldsymbol{v}}^{(3)} \text{ finite} \quad \text{at } \tilde{r} = 0. \tag{2.6}$$

If S_{ij} denotes the infinitely thin interface between fluids i and j the boundary conditions are

(i) continuity of tangential velocities

$$\tilde{v}_t^{(i)} = v_t^{(j)}, \tag{2.7}$$

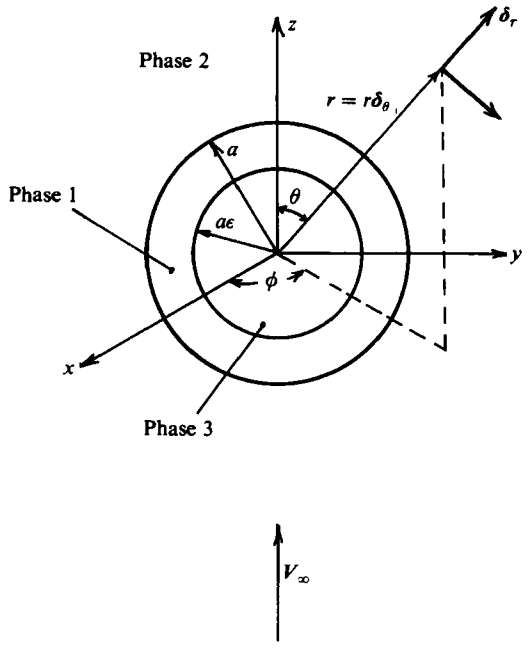

FIGURE 1. Coordinate system used in describing the flow around a perfectly symmetric type-A multiple drop.

(ii) vanishing of normal velocities

$$\tilde{v}_n^{(i)} = 0, \quad \tilde{v}_n^{(j)} = 0, \tag{2.8}$$

(iii) equilibrium between the applied loads, $\hat{\boldsymbol{n}} \cdot \tilde{\boldsymbol{T}}^{(i)} - \hat{\boldsymbol{n}} \cdot \tilde{\boldsymbol{T}}^{(j)}$, and the interfacial-stress resultants (e.g. Aris 1962)

$$\hat{\boldsymbol{n}} \cdot \tilde{\boldsymbol{T}}^{(i)} - \hat{\boldsymbol{n}} \cdot \tilde{\boldsymbol{T}}^{(j)} + \frac{\partial}{\partial \tilde{\boldsymbol{r}}_s} \cdot \tilde{\boldsymbol{\sigma}}^{(ij)} = 0. \tag{2.9}$$

Here $\partial/\partial \tilde{\boldsymbol{r}}_s$ is the surface gradient ($\partial/\partial \tilde{\boldsymbol{r}}_s = (\boldsymbol{\delta} - \hat{\boldsymbol{n}}\hat{\boldsymbol{n}}) \cdot \partial/\partial \tilde{\boldsymbol{r}}$), $\hat{\boldsymbol{n}}$ is the unit normal of S_{ij} (directed from the inner phase j to the outer phase i) and $\tilde{\boldsymbol{\sigma}}^{(i,j)}$ are the interfacial stresses.

A consequence of (2.9) is

$$\int_{S_{ij}} \mathrm{d}S \, [\hat{\boldsymbol{n}} \cdot \tilde{\boldsymbol{T}}^{(i)} - \hat{\boldsymbol{n}} \cdot \tilde{\boldsymbol{T}}^{(j)}] = 0. \tag{2.10}$$

By means of (2.4), this can be rewritten as

$$\hat{\boldsymbol{F}}^{(i)} - \hat{\boldsymbol{F}}^{(j)} + \int_{V_{ij}} \mathrm{d}V \left[\frac{\partial}{\partial \tilde{\boldsymbol{r}}} \tilde{\boldsymbol{\Phi}}^{(i)} - \frac{\partial}{\partial \tilde{\boldsymbol{r}}} \tilde{\boldsymbol{\Phi}}^{(j)} \right] = 0, \tag{2.11}$$

where V_{ij} denotes the volume enclosed by the surface S_{ij}. Here $\hat{\boldsymbol{F}}^{(i)}$ stands for the hydrodynamic or drag force. Equation (2.11) thus constitutes the appropriate force balance. For the special case in which the body force $\boldsymbol{f}^{(i)}$ is spatially constant, say $-\tilde{\boldsymbol{a}}^{(i)}$, (2.11) becomes

$$\hat{\boldsymbol{F}}^{(i)} - \hat{\boldsymbol{F}}^{(j)} + (\tilde{\boldsymbol{a}}^{(i)} - \tilde{\boldsymbol{a}}^{(j)}) \, V_{ij} = 0. \tag{2.12}$$

Quite clearly, the steady-state axisymmetric situation we consider is possible only if $\tilde{\boldsymbol{a}}^{(i)}$ is colinear with $\hat{\boldsymbol{k}}$, i.e. $\tilde{\boldsymbol{a}}^{(i)} = \alpha^{(i)} \hat{\boldsymbol{k}}$.

To make progress, the constitutive equation for the interface has to be specified. In the simplest case only an isotropic (interfacial) tension σ_{ij} is admitted:

$$\tilde{\boldsymbol{\sigma}}^{ij} = \sigma_{ij}(\boldsymbol{\delta} - \hat{\boldsymbol{n}}\hat{\boldsymbol{n}}). \tag{2.13}$$

Assuming in addition that σ_{ij} is constant leads to the two equations

$$\tilde{T}_{nt}^{(i)} = \tilde{T}_{nt}^{(j)}, \tag{2.14}$$

$$\tilde{T}_{nn}^{(i)} - \tilde{T}_{nn}^{(j)} = \tilde{K}_{ij}\sigma_{ij}, \tag{2.15}$$

with

$$\tilde{K}_{ij} = \frac{\partial}{\partial \tilde{\boldsymbol{r}}} \cdot \hat{\boldsymbol{n}} \tag{2.16}$$

the mean curvature of the surface S_{ij}.

Equations (2.1) supplemented by the boundary conditions (2.5)–(2.8), (2.14) and (2.15) constitute the set of equations one has to solve. Unfortunately, for a deformable particle like the multiple drop the interface S_{ij} is unknown *a priori* and has to be obtained simultaneously along with the solution of the problem.

To make progress analytically, serious approximation cannot be avoided. To this end we assume (*a*) that inertial effects are small and (*b*) that both interfacial tensions are so large that each of the two interfaces will never deviate much from spherical. This then dictates our method of approach: we shall apply the boundary conditions (2.5)–(2.8) and (2.14) at $S_{ij}^{(0)}$ (our initial guess for S_{ij}) to obtain a unique solution to the set of equations (2.1). Equation (2.15) is reserved to evaluate $\Delta S_{ij}^{(0)}$, i.e. the deviation of S_{ij} for our initial guess. Although one could – in principle – repeat that procedure with $S_{ij}^{(1)} = S_{ij}^{(0)} + \Delta S_{ij}^{(0)}$ as (improved) initial guess, we shall be content with $S_{ij}^{(1)}$. Phrased differently, we assume higher-order deformations $\Delta S_{ij}^{(l)} = S_{ij}^{(l+1)} - S_{ij}^{(l)}$ ($l > 1$) to be small in comparison with first-order deformation $\Delta S_{ij}^{(1)}$.

Before calculating $\Delta S_{ij}^{(1)}$ it seems advantageous to introduce dimensionless quantities:

$$\left.\begin{aligned} \boldsymbol{r} = \tilde{\boldsymbol{r}}/a, \quad \boldsymbol{v}^{(i)} = \tilde{\boldsymbol{v}}^{(i)}/v_\infty, \\ p^{(i)} = \frac{\hat{p}^{(i)}\, a}{v_\infty \eta^{(i)}}, \quad \boldsymbol{T}^{(i)} = \frac{a}{v_\infty \eta^{(i)}}\, \hat{\boldsymbol{T}}^{(i)}, \\ \boldsymbol{a}^{(i)} = \tilde{\boldsymbol{a}}^{(i)}/\alpha^{(i)} = \hat{\boldsymbol{k}}. \end{aligned}\right\} \tag{2.17}$$

The relevant equations now read

$$\left.\begin{aligned} \frac{\partial}{\partial \boldsymbol{r}} \cdot \boldsymbol{v}^{(i)} = 0, \\ Re^{(i)}\, \boldsymbol{v}^{(i)} \cdot \frac{\partial}{\partial \boldsymbol{r}}\, \boldsymbol{v}^{(i)} = -\frac{\partial}{\partial \boldsymbol{r}}\, p^{(i)} + \nabla^2 \boldsymbol{v}^{(i)}, \end{aligned}\right\} \tag{2.18}$$

subject to the boundary conditions (to dominant order)

$$\boldsymbol{v}^{(2)} \to \hat{\boldsymbol{k}} \quad \text{as } r \to \infty,$$

$$\boldsymbol{v}^{(3)} \text{ finite} \quad \text{at } r = 0,$$

$$\left.\begin{aligned} \boldsymbol{v}^{(i)} = \boldsymbol{v}^{(j)}, \\ v_r^{(i)} = 0, \\ T_{r\theta}^{(j)} = \eta_{ij}\, T_{r\theta}^{(i)} \end{aligned}\right\} \quad \text{at each spherical interface } S_{ij}^{(0)}. \tag{2.19}$$

Here

$$Re^{(i)} = \frac{\rho^{(i)} v_\infty a}{\eta^{(i)}} \tag{2.20a}$$

denotes the Reynolds number of region i,

$$\eta_{ij} = \eta^{(i)}/\eta^{(j)}, \tag{2.20b}$$

is the viscosity ratio and (for later use)

$$\rho_{ij} = \rho^{(i)}/\rho^{(j)} \tag{2.20c}$$

is the density ratio.

If the mean curvature $\tilde{K}_{ij}$ is scaled with the radius r_{ij} of the sphere (corresponding to $S_{ij}^{(0)}$) in question, the first-order deformation of the 2–1 interface is governed by

$$\lambda_{21}\left[T_{rr}^{(2)} - \eta_{12} T_{rr}^{(1)} + \frac{a^2(\alpha^{(2)} - \alpha^{(1)})}{v_\infty \eta^{(2)}} P_1(\mu)\right] = K_{21}, \tag{2.21}$$

and similarly, for the 1–3 interface,

$$\epsilon\lambda_{31}\left[T_{rr}^{(1)} - \eta_{31} T_{rr}^{(3)} + \frac{\epsilon a^2(\alpha^{(1)} - \alpha^{(3)})}{v_\infty \eta^{(1)}} P_1(\mu)\right] = K_{13}. \tag{2.22}$$

Here

$$\lambda_{ij} = \frac{v_\infty \eta^{(i)}}{\sigma_{ij}}$$

denotes the capillary number,

$$\mu = \cos\theta, \quad K_{21} = a\tilde{K}_{21}, \quad K_{13} = a\epsilon\tilde{K}_{13}, \tag{2.23}$$

and $P_n(\mu)$ denotes the Legendre polynomial of degree n.

For completeness we also list the balance equations (2.12). With

$$\hat{\boldsymbol{F}}^{(i)} = \hat{F}^{(i)}\boldsymbol{k} = a v_\infty \eta^{(i)} F^{(i)}\boldsymbol{k}, \tag{2.24}$$

the force balances (2.12) become

$$F^{(2)} - \eta_{12} F^{(1)} + \tfrac{4}{3}\pi \frac{a^2(\alpha^{(2)} - \alpha^{(1)})}{v_\infty \eta^{(2)}} = 0, \tag{2.25}$$

and

$$F^{(1)} - \eta_{31} F^{(3)} + \tfrac{4}{3}\pi\epsilon^3 \frac{a^2(\alpha^{(1)} - \alpha^{(3)})}{v_\infty \eta^{(1)}} = 0. \tag{2.26}$$

3. The creeping-motion limit

As long as the Reynolds numbers $Re^{(i)}$ for each region are sufficiently small it makes sense to neglect inertia altogether, as a first approximation, i.e. to set $Re^{(i)} = 0$ in the equations of motion (2.18). Attaching a subscript 0 to the velocity and pressure fields to indicate the creeping-motion limit, we have for $(\boldsymbol{v}_0^{(i)}, p_0^{(i)})$

$$v_{r0}^{(i)} = -[A_2^{(i)} + B_2^{(i)} r^{-3} + C_2^{(i)} r^2 + D_2^{(i)} r^{-1}] P_1(\mu), \tag{3.1a}$$

$$v_{\theta 0}^{(i)} = [2A_2^{(i)} - B_2^{(i)} r^{-3} + 4C_2^{(i)} r^2 + D_2^{(i)} r^{-1}] \frac{J_2(\mu)}{(1-\mu^2)^{\frac{1}{2}}}, \tag{3.1b}$$

$$p_0^{(i)} = \Pi_0^{(i)} - [10C_2^{(i)} r + D_2^{(i)} r^{-2}] P_1(\mu). \tag{3.1c}$$

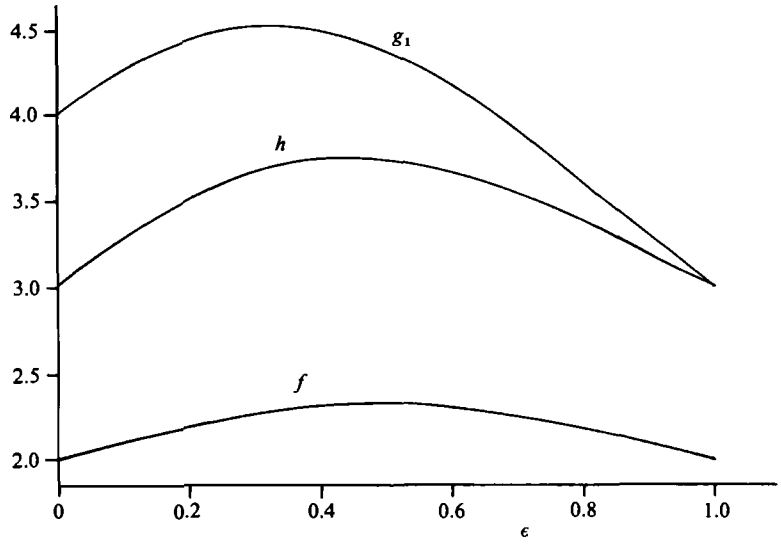

FIGURE 2. The functions f, g_1 and h as defined by (2.9) and (2.12).

The functions J_n are the Gegenbauer functions of order n and degree $-\frac{1}{2}$ and $\Pi_0^{(i)}$ is a constant. Since at large distances from the sphere the velocity has to be equal to $\hat{\boldsymbol{k}}$, the free-stream velocity, and since it has to be finite at the centre of the particle, we know that

$$A_2^{(2)} = -1, \quad C_2^{(2)} = 0, \quad B_2^{(3)} = D_2^{(3)} = 0. \tag{3.2}$$

Equations (3.1) imply

$$T_{rr0}^{(i)} = -\Pi_0^{(i)} + 6[B_2^{(i)} r^{-4} + C_2^{(i)} r + \tfrac{1}{2} D_2^{(i)} r^{-2}] P_1(\mu), \tag{3.3a}$$

$$T_{r\theta 0}^{(i)} = 6[B_2^{(i)} r^{-4} + C_2^{(i)} r] \frac{J_2(\mu)}{(1-\mu^2)^{\frac{1}{2}}}. \tag{3.3b}$$

As a consequence the hydrodynamic force $F_0^{(i)}$ is given by

$$F_0^{(i)} = 4\pi D_2^{(i)}. \tag{3.4}$$

To determine the eight unknown coefficients $B_2^{(2)}$, $D_2^{(2)}$, $A_2^{(1)}$, $B_2^{(1)}$, $C_2^{(1)}$, $D_2^{(1)}$, $A_2^{(1)}$ and $C_2^{(3)}$ we use the eight boundary conditions (2.19) and $S_{ij}^{(0)}$, i.e. at the two surfaces $r = 1$ and $r = \epsilon$ respectively. The result for $D_2^{(2)}$ is†

$$D_2^{(2)} = \frac{3}{2} - \frac{1-\epsilon}{K} [\eta_{13} f(\epsilon) + \tfrac{1}{2}(1-\epsilon) g_1(\epsilon)], \tag{3.5}$$

with

$$K = 4\eta_{12}\eta_{13} + 2\eta_{13}(1+\eta_{32})(1-\epsilon) f + (1-\epsilon)^2 g_1. \tag{3.6}$$

In these equations f and g_1 are positive-valued functions of ϵ, listed explicitly in Appendix A and plotted in figure 2. Although $D_2^{(2)}$ is a function not only of ϵ but of the various viscosity ratios as well, it can be shown rigorously that it is monotonically increasing with increasing ϵ (η_{12}, η_{13} fixed),

$$\lim_{\epsilon \to 0} D_2^{(2)} = \frac{2+3\eta_{12}}{2(1+\eta_{12})} \leqslant D_2^{(2)} \leqslant \tfrac{3}{2} = \lim_{\epsilon \to 1} D_2^{(2)}. \tag{3.7}$$

† This is in perfect agreement with a recent result of Rushton & Davies (1983).

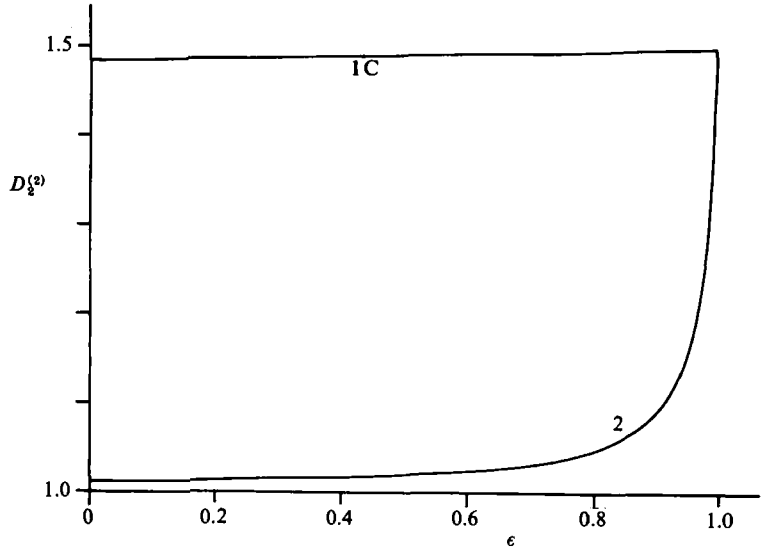

FIGURE 3. The particle drag coefficient $D_2^{(2)}$ as a function of ϵ for the systems 1C and 2 of table 1.

Thus the drag force on the particle is larger than that for a droplet of viscosity $\eta^{(1)}$ and less than the drag force for a rigid sphere (see also figure 3). To understand why the rigid-sphere limit results for very thin liquid membranes, a look at the streamlines is helpful. As shown in figure 4, the steady-state conditions require an internal circulation to be set up such that the direction of the streamlines in the inner region are reversed compared to that in a single fluid droplet. As ϵ approaches one, all internal circulation is suppressed, since otherwise the fluid would have to change directions over the vanishingly small distance $(1-\epsilon)a$. Thus in the $\epsilon \to 1$ limit the multiple drop consists of a stationary fluid encapsulated by an immobile fluid shell, so that it behaves like a solid sphere.† In that case mass and heat transfer from the inner drop to the solvent (and vice versa) will thus be by diffusion alone.

Since the hydrodynamic force exerted by the liquid shell upon the inner droplet is related to $D_2^{(1)}$, it seems worthwhile to list that result too:

$$D_2^{(1)} = -\frac{\epsilon}{(1-\epsilon)K}[2\eta_{13} + (1-\epsilon)h(\epsilon)]. \tag{3.8}$$

The positive-valued function h depends only upon ϵ (see Appendix A), and is shown in figure 2. The fact that $D_2^{(1)}$ is strictly non-positive can be explained by reference to the streamline pattern of figure 3. For fixed viscosity ratios, $D_2^{(1)}$ decreases monotonically from its $\epsilon = 0$ limit of zero to $-[2\eta_{12}(1-\epsilon)]^{-1}$ for $\epsilon \to 1$ (see also figure 5). Note that for infinitely thin shells ($\epsilon \to 1$) membrane stresses are involved, which, for a liquid membrane, involve the membrane viscosity $\eta^{(1)}(1-\epsilon)a$ rather than $\eta^{(1)}$. It is for this reason, and our way of non-dimensionalizing, that all coefficients that characterize the shell region blow up like $(1-\epsilon)^{-1}$ for $\epsilon \to 1$.

All the other coefficients are of no direct concern to us, and we refer to Appendix A, which lists explicitly all coefficients of the creeping-motion solution. With $(\boldsymbol{v}_0, p_0)$

† The same conclusion can also be reached from dimensional reasoning alone.

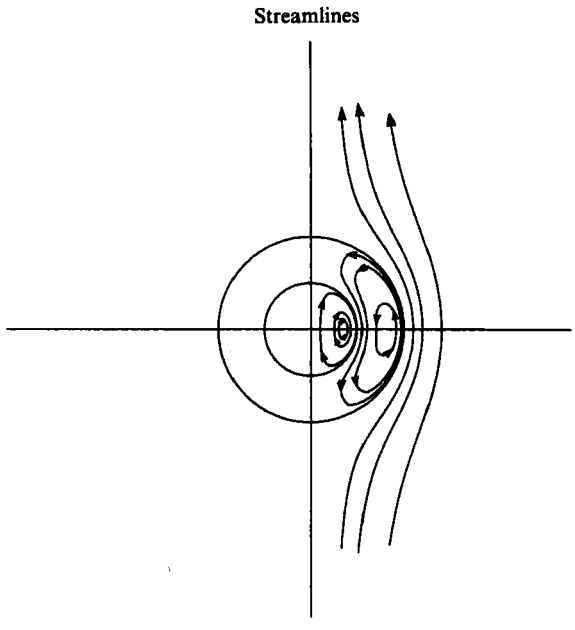

FIGURE 4. The creeping-motion streamline pattern for a type-A multiple droplet.

known in all regions, we next turn to the normal stresses to see whether or not the interfaces remain spherical.

As far as the 2–1 interface is concerned, we turn to (2.21). Explicitly it reads

$$\lambda_{21}(-\Pi_0^{(2)}+\eta_{12}\Pi_0^{(1)})+\left[3(D_2^{(2)}-D_2^{(1)})+\frac{a^2(\alpha^{(2)}-\alpha^{(1)})}{v_\infty \eta^{(2)}}\right]P_1(\mu)=K_{21}, \tag{3.9}$$

where use has been made of (3.3a, b) and the continuity of the tangential stresses has been employed. It is clear from (3.4) that the term multiplying $P_1(\mu)$ in (3.9) is nothing but the force balance (2.25). Consequently, (3.9) reduces to

$$\lambda_{21}(-\Pi_0^{(2)}+\eta_{12}\Pi_0^{(1)})=K_{21}. \tag{3.10}$$

This implies that the mean curvature is identically constant, i.e. the outer surface remains undeformed ($K_{21}=2$). Thus, after putting (without loss of generality) $\Pi_0^{(2)}$ equal to zero, we have

$$\Pi_0^{(1)}=2\frac{\eta_{21}}{\lambda_{21}}=2\frac{\sigma_{21}}{v_\infty \eta^{(1)}}. \tag{3.11}$$

By the same token, the inside surface (1–3) does not deform either. Explicitly we find that the pressure difference between the inside and the membrane is given by

$$2=\epsilon\lambda_{13}(-\Pi_0^{(1)}+\eta_{31}\Pi_0^{(3)}). \tag{3.12}$$

Under creeping-flow conditions none of the surfaces deform, irrespective of the magnitude of the capillary number. Deformation is a nonlinear effect, and for Newtonian fluids inertia is the only source of nonlinearity.

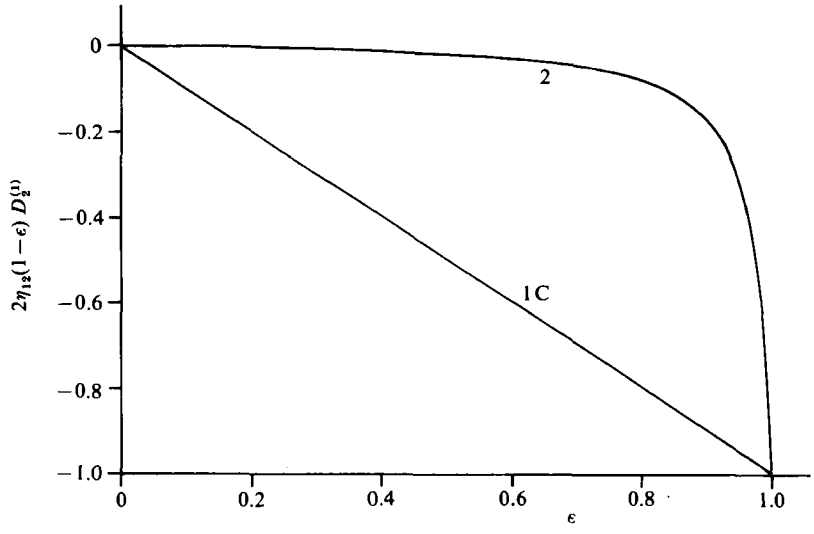

FIGURE 5. The scaled inner-droplet drag coefficient $D_2^{(1)}$ as a function of ϵ for systems 1C and 2 of table 1.

4. Inertial effects

Inertial effects will be small whenever $Re^{(i)}$, the Reynolds number (based on a) in region i is small. This implies that inside the particle (i.e. in regions 3 and 1) the equations of motion

$$Re^{(i)}\,\boldsymbol{v}^{(i)}\cdot\frac{\partial}{\partial \boldsymbol{r}}\,\boldsymbol{v}^{(i)} = -\frac{\partial}{\partial \boldsymbol{r}}\,p^{(i)} + \nabla^2\boldsymbol{v}^{(i)} \tag{4.1}$$

can be solved by means of a regular perturbation expansion

$$\left.\begin{aligned} \boldsymbol{v}^{(i)} &= \boldsymbol{v}_0^{(i)} + Re^{(i)}\,\boldsymbol{v}_{11}^{(i)} + \ldots, \\ p^{(i)} &= p_0^{(i)} + Re^{(i)}\,p_{11}^{(i)} + \ldots, \end{aligned}\right\} \tag{4.2}$$

where the fields $(\boldsymbol{v}_{11}^{(i)}, p_{11}^{(i)})$ satisfy

$$\boldsymbol{v}_0^{(i)}\cdot\frac{\partial}{\partial \boldsymbol{r}}\,\boldsymbol{v}_0^{(i)} = -\frac{\partial}{\partial \boldsymbol{r}}\,p_{11}^{(i)} + \nabla^2\boldsymbol{v}_{11}^{(i)}. \tag{4.3}$$

Utilizing (3.1), a particular solution of (4.3) is

$$\left.\begin{aligned} p_{11p}^{(i)} &= I_{1p}^{(i)}(r)\,P_2(\mu) + I_{2p}^{(i)}(r), \\ v_{r11p}^{(i)} &= H_p^{(i)}(r)\,P_2(\mu), \\ v_{\theta 11p}^{(i)} &= K_p^{(i)}(r)\,\frac{J_3(\mu)}{(1-\mu^2)^{\frac{1}{2}}}, \end{aligned}\right\} \tag{4.4}$$

with

$$\begin{aligned} I_{1p}^{(i)} = B_2^{(i)}[-3C_2^{(i)}\,r^{-1} - A_2^{(i)}\,r^{-3} - \tfrac{1}{4}B_2^{(i)}\,r^{-6}] \\ - C_2^{(i)}[A_2^{(i)}\,r^2 + \tfrac{2}{3}C_2^{(i)}\,r^4] + D_2^{(i)}[-\tfrac{11}{6}C_2^{(i)}\,r + \tfrac{1}{3}D_2^{(i)}\,r^{-2} - B_2^{(i)}\,r^{-4}], \end{aligned} \tag{4.5a}$$

$$I_{2p}^{(i)} = B_2^{(i)}[2C_2^{(i)} r^{-1} - \tfrac{1}{4}B_2^{(i)} r^{-6}] + \tfrac{1}{6}C_2^{(i)2} r^4 + D_2^{(i)}[-\tfrac{2}{3}C_2^{(i)} r - \tfrac{1}{12}D_2^{(i)} r^{-2} - \tfrac{1}{4}B_2^{(i)} r^{-6}], \quad (4.5b)$$

$$H_p^{(i)} = \tfrac{1}{4}D_2^{(i)}[A_2^{(i)} - B_2^{(i)} r^{-3} - C_2^{(i)} r^2 + D_2^{(i)} r^{-1}], \quad (4.5c)$$

$$K_p^{(i)} = D_2^{(i)}[-\tfrac{1}{2}A_2^{(i)} - \tfrac{1}{4}B_2^{(i)} r^{-3} + C_2^{(i)} r^2 - \tfrac{1}{4}D_2^{(i)} r^{-1}]. \quad (4.5d)$$

It is interesting to see that in the inside region (region 3) the functions $H_p^{(3)}$ and $K_p^{(3)}$ vanish identically. This implies that the full Navier–Stokes equations are satisfied by the fields $(\boldsymbol{v}_0^{(3)}, p_0^{(3)} + Re^{(3)} p_1)$, i.e. that only the pressure is affected by inertia. In our case, regions 1 and 2 (the shell and continuous fluid phase respectively) require small inertial effects, so that (4.2) are restricted to $Re^{(i)} < 1$, $i = 1, 2$. Supplemented by the general solution to the homogeneous equation (4.3), the fields $(\boldsymbol{v}_{11}^{(i)}, p_{11}^{(i)})$ are known. In order to get some information about the necessary homogeneous terms, we turn to region 2. It is well established that close to the sphere, i.e. for r less than some critical distance r_c of order $1/Re^{(2)}$, a regular perturbation like the one just used for the inside regions still works. Outside this region, i.e. for $r < r_c$, inertia dominates. Scaling distances in this outer region with r_c (the particle appears as a 'point'), i.e. introducing

$$\rho = r/r_c = r\,Re^{(2)}, \quad (4.6)$$

gives the Oseen equation. For the axisymmetric case under consideration, the general solution is known (Lamb 1932). Denoting by v_ρ and v_θ the components of $\boldsymbol{V}$, the velocity according to Oseen's equation, we deduce the $\rho \ll 1$ behaviour of $\boldsymbol{V}$ to be

$$v_\rho \to \left\{1 + Re^{(2)}\left[-\frac{1}{\rho}B_0 + \tfrac{1}{4}B_0\right]\right\} P_1(\mu) - Re^{(2)}\frac{B_0}{4}P_2(\mu) + o(Re^{(2)}), \quad (4.7a)$$

$$v_\theta \to \left\{-2 + Re^{(2)}\left[\frac{1}{\rho}B_0 - \tfrac{1}{2}B_0\right]\right\} \frac{J_2(\mu)}{(1-\mu^2)^{\frac{1}{2}}} + Re^{(2)}\frac{B_0}{2}\frac{J_3(\mu)}{(1-\mu^2)^{\frac{1}{2}}} + o(Re^{(2)}). \quad (4.7b)$$

Comparing with the inner solution $\boldsymbol{v}_0^{(2)}$ for $r \gg 1$ determines B_0:

$$B_0 = D_2^{(2)}. \quad (4.8)$$

With B_0 determined, (4.7) suggests that (3.2) be rewritten as

$$\boldsymbol{v}^{(i)} = [1 + \tfrac{1}{4}Re^{(2)} D_2^{(2)}]\,\boldsymbol{v}_0^{(i)} + Re^{(i)}\,\boldsymbol{v}_1^{(i)} + \ldots, \quad (4.9a)$$

$$p^{(i)} = [1 + \tfrac{1}{4}Re^{(2)} D_2^{(2)}]\,p_0^{(i)} + Re^{(i)}\,p_1^{(i)} + \ldots, \quad (4.9b)$$

with $(\boldsymbol{v}_1^{(i)}, p_1^{(i)})$ of the form (recall (4.4))

$$p_1^{(i)} = I_1^{(i)}(r)\,P_2(\mu) + I_2^{(i)}(r), \quad (4.10a)$$

$$v_{r1}^{(i)} = H^{(i)}(r)\,P_2(\mu), \quad (4.10b)$$

$$v_{\theta 1}^{(i)} = K^{(i)}(r)\frac{J_3(\mu)}{(1-\mu^2)^{\frac{1}{2}}} \quad (4.10c)$$

subject to the boundary conditions

$$H^{(2)}(\infty) = -\tfrac{1}{4}D_2^{(2)}, \quad (4.11a)$$

$$K^{(2)}(\infty) = \tfrac{1}{2}D_2^{(2)}. \quad (4.11b)$$

Utilizing now the general solution of the Stokes equation given by Happel & Brenner (1973), the functions appearing in (4.10) are

$$I_1^{(i)}(r) = I_{1p}^{(i)}(r) - [7C_3^{(i)} r^2 + 2D_3^{(i)} r^{-3}], \tag{4.12a}$$

$$I_2^{(i)}(r) = \Pi_2^{(i)} + I_{2p}^{(i)}(r), \tag{4.12b}$$

$$H^{(i)}(r) = H_p^{(i)}(r) - [A_3^{(i)} r + B_3^{(i)} r^{-4} + C_3^{(i)} r^3 + D_3^{(i)} r^{-2}], \tag{4.12c}$$

$$K^{(i)}(r) = K_p^{(i)}(r) + [3A_3^{(i)} r - 2B_3^{(i)} r^{-4} + 5C_3^{(i)} r^3]. \tag{4.12d}$$

Since $A_2^{(2)} = -1$, the boundary conditions (4.11) are automatically satisfied by H_p and K_p. This implies

$$A_3^{(2)} = 0, \quad C_3^{(2)} = 0, \tag{4.13a}$$

while finiteness at the centre requires

$$B_3^{(3)} = 0, \quad D_3^{(3)} = 0. \tag{4.13b}$$

The remaining eight coefficients $B_3^{(2)}$, $D_3^{(2)}$, $A_3^{(1)}$, $B_3^{(1)}$, $C_3^{(1)}$, $D_3^{(1)}$, $A_3^{(3)}$ and $C_3^{(3)}$ are determined by means of the same boundary conditions used previously in the creeping-flow limit.

It is readily checked that the fields $(\boldsymbol{v}_1^{(i)}, p_1^{(1)})$ of the form (4.10) do not give rise to any forces $\boldsymbol{F}_1^{(i)}$. This implies that the dimensional drag force exerted upon the particle is given by

$$\hat{\boldsymbol{F}}^{(2)} = 4\pi\eta^{(2)} a v_\infty D_2^{(2)} [1 + \tfrac{1}{4} Re^{(2)} D_2^{(2)} + o(Re^{(2)})] \hat{\boldsymbol{k}}. \tag{4.14}$$

Since it is physically clear that $D_2^{(2)}$ has to be positive, we see that inertia always increases the drag, as expected.

By the same token, the dimensional drag force exerted by the liquid shell on the inside fluid is

$$\hat{\boldsymbol{F}}^{(1)} = 4\pi\eta^{(1)} a v_\infty D_2^{(1)} [1 + \tfrac{1}{4} Re^{(2)} D_2^{(2)} + o(Re^{(1)})] \hat{\boldsymbol{k}}. \tag{4.15}$$

Thus to this order of approximation the ratio of the drag forces

$$\hat{F}^{(2)} / \hat{F}^{(1)} = \eta_{12} D_2^{(2)} / D_2^{(1)} \tag{4.16}$$

is the same as in the creeping-motion limit. Higher-order inertia effects and/or explicitly taking the deformation into account are needed in order for this ratio to become dependent upon particle size a.

To see whether the particle does deform, it is sufficient to concentrate solely on the fields $(\boldsymbol{v}_1^{(i)}, p_1^{(i)})$. Proceeding as before, it can be shown that the normal component of the stress vector $t_1^{(i)} = \hat{\boldsymbol{n}} \cdot \boldsymbol{T}_1^{(i)}$ is of the form

$$t_{r1}^{(i)} = \alpha^{(i)} + \beta^{(i)} P_2(\mu), \tag{4.17}$$

with

$$\beta^{(i)}(r) = 2H^{(i)\prime}(r) - I_1^{(i)}(r). \tag{4.18}$$

The prime indicates an ordinary derivative. The first term (involving the αs) is of no concern, since, in conjunction with (3.10), it merely allows us to determine the pressure constants $\Pi_1^{(i)}$. With a term proportional to P_2 appearing now in (2.21) and (2.22), each interface deforms into a spheroid, i.e.

$$r_0 = 1 + \delta_{20} P_2(\mu), \tag{4.19a}$$

$$r_1 = \epsilon(1 + \delta_{21} P_2(\mu)), \tag{4.19b}$$

with†
$$\left.\begin{aligned}\delta_{20} &= \tfrac{1}{4}\,We^{(2)}[\beta^{(2)}(1)-\rho_{12}\,\beta^{(1)}(1)],\\ \delta_{2i} &= \tfrac{1}{4}\epsilon\,We^{(1)}[\beta^{(1)}(\epsilon)-\rho_{31}\,\beta^{(3)}(\epsilon)]\end{aligned}\right\} \tag{4.20a}$$

$$\rho_{ij} = \rho^{(i)}/\rho^{(j)}. \tag{4.20b}$$

Here
$$We^{(i)} = Re^{(i)}\,\lambda_{ij} = \frac{a v_\infty^2\,\rho^{(i)}}{\sigma_{ij}} \tag{4.21}$$

denotes the Weber number in region (i). The requirement that each deformation be small requires $We^{(2)}$ and $We^{(1)}$ to be small. We should emphasize at this point that We is proportional to v_∞^2, so that the deformation is proportional to v_∞^2 for $v_\infty \to 0$. This clearly illustrates the nonlinearity of the effect.

Explicit expressions for δ_{20} and δ_{2i} are listed in Appendix B. It follows from these results that for $\epsilon \to 0$, δ_{2i} tends to zero (linearly in ϵ), while δ_{20} becomes

$$\lim_{\epsilon\to 0}\delta_{20} = \tfrac{1}{4}We^{(2)}\,\frac{1}{(1+\eta_{12})^3}\{\tfrac{1}{12}\rho_{12}(1+\eta_{12})-[\tfrac{5}{6}+\tfrac{319}{120}\eta_{12}+\tfrac{57}{20}\eta_{12}^2+\tfrac{81}{80}\eta_{12}^3]\}. \tag{4.22}$$

This is the well-known result for a droplet (Taylor & Acrivos 1964). In the opposite limit $\epsilon \to 1$, (4.20a, b) imply

$$\left.\begin{aligned}\delta_{20} &\to -\tfrac{1}{16}We^{(2)}(1-\epsilon)^{-1},\\ \delta_{2i} &\to -\frac{\sigma_{21}}{\sigma_{13}}\,\delta_{20}.\end{aligned}\right\} \tag{4.23}$$

For $\epsilon \to 1$ the characteristic lengthscale for region 1 has to be the membrane thickness $a(1-\epsilon)$. Consequently the appearance of a factor $1-\epsilon$ in (4.23) was to be expected. What is unexpected – and physically inadmissible – is the fact that δ_{20} and δ_{2i} are not equal for $\epsilon \to 1$. This implies that, as far as the deformation is concerned, our results do not allow us to take the $\epsilon \to 1$ limit. If we postulate the continuum concept down to $\epsilon \to 1$, then for $\epsilon \approx 1$ our scaling process no longer works, since the membrane thickness $1-\epsilon$ enters as an independent lengthscale (Johnson & Sadhal 1983). High 'lubrication' pressures $p^{(1)}$ would have to be reckoned with, a concept neglected in the present study.

Since the expressions for the deformations δ_{20} and δ_{2i} are so complicated, general statements are almost impossible to make. Table 1 lists a number of systems (taken from the literature) that we have studied. Systems 2, 5A, 6A and 6B are characterized by a large solvent viscosity ($\eta_{12} \leqslant 10^{-1}$, $\eta_{32} \lesssim 10^{-3}$). As a consequence, all coefficients (from $A_2^{(1)}$ to $D_3^{(3)}$) change rather rapidly for ϵ close to one (see also figures 2 and 5). In this ϵ-range the functions δ_{20} and δ_{2i} for these systems show rather large and almost erratic changes. For system 6A this happens in the range $0.97 < \epsilon < 1$. For smaller ϵ, δ_{20} is strictly negative (oblate spheroid), while δ_{2i} twice changes sign: once for ϵ close to zero, where δ_{2i} first becomes negative, and a second time at some intermediate ϵ, where it again becomes positive (prolate spheroid). For system 6A the corresponding ϵ-values are 0.01 and 0.14 respectively. The magnitude of δ_{2i} is small over the whole range before the fluctuations occur. It is interesting to see that none of these systems has been observed in the perfectly symmetric type-A configuration envisioned by us.

† The mean curvature of a particle of the form $r = 1+\Sigma_n\,\delta_n P_n$ is

$$K = 2+\sum_n (n(n+1)-2)\,\delta_n P_n + O(\delta^2).$$

†	Phase (region)	ρ (g/cm^3)	η (g cm^{-1} s^{-1})	σ (dyn/cm)	Preparation	cut-point ϵ^*
Type O/W/O (Group 1)						
System 1A	(1) water, SDDS (0.2% wt) (a surfactant)	9.98×10^{-1}	1.00×10^{-2}	$\sigma_{21}=7.0$	double emulsion	$\epsilon^*=5.3\times10^{-1}$
	(2) *o*-xylene	8.81×10^{-1}	7.60×10^{-3}			
	(3) hexane, toluene, benzene (33% wt each)	8.01×10^{-1}	5.11×10^{-3}	$\sigma_{13}=7.0$		
System 1B	(1) water, glycerol (30% wt), SDDS (0.2% wt)	1.07	2.46×10^{-2}	$\sigma_{21}=$ N/A‡	double emulsion	$\epsilon^*=6.3\times10^{-1}$
	(2) *o*-xylene	8.81×10^{-1}	7.60×10^{-3}			
	(3) hexane, toluene, benzene (33% wt each)	8.01×10^{-1}	5.11×10^{-3}	$\sigma_{13}=$ N/A		
System 1C	(1) water, glycerol (70% wt), SDDS (0.2% wt)	1.18	2.22×10^{-1}	$\sigma_{21}=$ N/A	double emulsion	$\epsilon^*=7.0\times10^{-1}$
	(2) *o*-xylene	8.81×10^{-1}	7.60×10^{-3}			
	(3) hexane, toluene, benzene (33% wt each)	8.01×10^{-1}	5.11×10^{-3}	$\sigma_{21}=$ N/A		
Type W/O/W (Group 2)						
System 2	(1) mineral oil, span 80 (10% vol.)	8.79×10^{-1}	2.53	$\sigma_{21}=4.0$	double emulsion	$\epsilon^*=1.7\times10^{-1}$
	(2) corn syrup (type B)	1.40	1.10×10^{2}			$\epsilon^*=8.8\times10^{-1}$
	(3) water, glycerol (50% wt)	1.14	8.35×10^{-2}	$\sigma_{13}=$ N/A		
Type W/O/W (Group 3)						
System 3	(1) *silicone oil, span* 80 (3% vol.)	9.72×10^{-1}	1.26×10^{2}	$\sigma_{21}=$ N/A	double emulsion	$\epsilon^*=8.4\times10^{-1}$
	(2) water, phenol (0.63 mM, 0.006% wt)	9.98×10^{-1}	1.00×10^{-2}			
	(3) water, NaOH (0.1 N, 0.4% wt)	1.00	1.02×10^{-2}	$\sigma_{13}=$ N/A		
Type W/O/W (Group 4)						
	(1) isopropyl myristate, Span 80 (5% wt)	8.53×10^{-1}	5.61×10^{-2}	$\sigma_{21}=$ N/A	double emulsion	$\epsilon^*=1.00$
	(2) water	9.98×10^{-1}	1.00×10^{-2}			
	(3) water, lauryl ether (2.0% wt) (a surfactant)	9.98×10^{-1}	1.00×10^{-2}	$\sigma_{13}=$ N/A		
Type A/W/O (Group 5)						
System 5A	(1) water	1.00	1.00×10^{-2}	$\sigma_{21}=32.0$	diffusion column	$\epsilon^*=2.5\times10^{-1}$
	(2) mineral oil, Varsol (sample I)	7.80×10^{-1}	9.36×10^{-3}			
	(3) air	1.20×10^{-3}	1.81×10^{-4}	$\sigma_{13}=72.0$		
System 5B	(1) water	1.00	1.00×10^{-2}	$\sigma_{21}=32.0$	diffusion column	$\epsilon^*=4.0\times10^{-2}$
	(2) mineral oil, Varsol (sample V)	8.60×10^{-1}	4.73×10^{-1}			
	(3) air	1.20×10^{-3}	1.81×10^{-4}	$\sigma_{13}=72.0$		
Type A/W/O (Group 6)						
System 6A	(1) Freon (R113)	1.58	7.30×10^{-3}	$\sigma_{21}=46.0$	diffusion column	$\epsilon^*=1.5\times10^{-1}$
	(2) water, glycerol (46.4% wt)	1.12	5.06×10^{-2}			
	(3) air	1.20×10^{-3}	1.81×10^{-4}	$\sigma_{13}=19.0$		
System 6B	(1) Freon (R113)	1.58	7.30×10^{-3}	$\sigma_{21}=29.0$		
	(2) water, glycerol (98.8% wt)	1.25	1.17×10^{1}		diffusion column	$\epsilon^*=1.0\times10^{-2}$
	(3) air	1.20×10^{-3}	1.18×10^{-4}	$\sigma_{13}=19.0$		

† Group (1) Li (1971); (2) Ulbrecht *et al.* (1982); (3) Halwachs *et al.* (1980); (4) Florence & Whitehill (1981); (5) Mercier *et al.* (1974); (6) Mori *et al.* (1977).

‡ N/A ≡ not available.

TABLE 1. Systems used

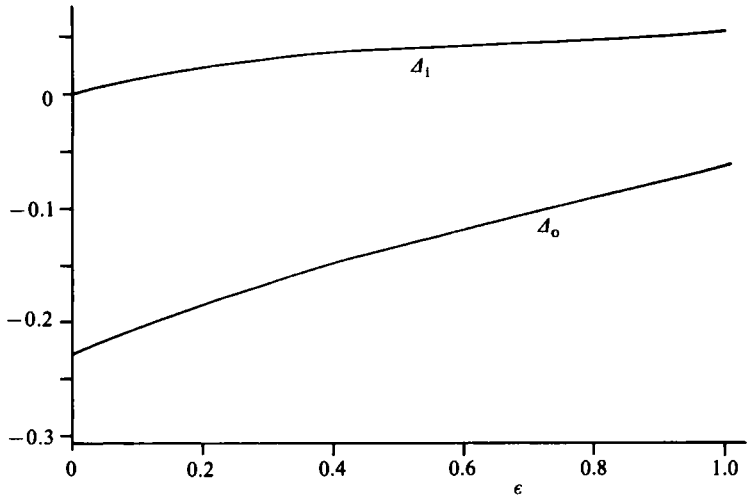

FIGURE 6. The outside and inside deformation parameters

$$\Delta_o = \frac{(1-\epsilon)}{We^{(2)}}\,\delta_{2o}, \quad \Delta_i = \frac{(1-\epsilon)}{We^{(1)}}\,\delta_{2i}$$

for system 1A.

For systems 5 and 6 a diffusion column was used, and the corresponding Reynolds numbers are rather large (see §1). The encapsulating liquid was observed to be concentrated on the rear of the inside bubble. System 2, on the other hand, is not of type A, but rather of type B (Ulbrecht, Stroeve & Prabodh 1980). We included it – as well as the other type-B system (system 3) – in the table in order to see whether our hydrodynamic results would somehow enable us to discriminate between type-A and type-B or type-C multiple drops.

For all other systems of table 1 the deformations are not only one-sided, but of the same type too. The outside deforms into an oblate spheroid and the inside into a prolate one. Figure 6, based on the data of system 1A, actually is typical for all other systems too. The shape of the deformed particle is shown in figure 7. It is apparent from these graphs that the shell thickness is least at the poles, which would thus be likely points for rupture. If we put

$$\delta_{2o} = We^{(2)}\,\delta_{2o}, \quad \delta_{2i} = We^{(1)}\,\delta_{2i}. \tag{4.24}$$

The condition for rupture ($r_o = r_i$) reads

$$1-\epsilon = We^{(2)}\left\{-\delta_{2o} + \epsilon\,\frac{We^{(1)}}{We^{(2)}}\,\delta_{2i}\right\}. \tag{4.25}$$

If ϵ_c denotes the point of intersection of the right- and left-hand sides of this equation then the dependence of ϵ_c on particle size is seen to reside in the Weber number. Increasing the particle size requires smaller and smaller values of ϵ in order for type-A droplets to exist (see figure 8). Li's (1971) observation that decreasing the droplet size greatly stabilized the droplets may be due (at least partly) to this effect. Alternatively, if multiple drops do exist, with a volume ratio V_m/V_i of encapsulating fluid relative to the inside volume of less than $(1-\epsilon_c^3)/\epsilon_c^3$, then these drops can never be symmetric type-A droplets. Multiple drops generated in a diffusion column all seem to fall into that category.

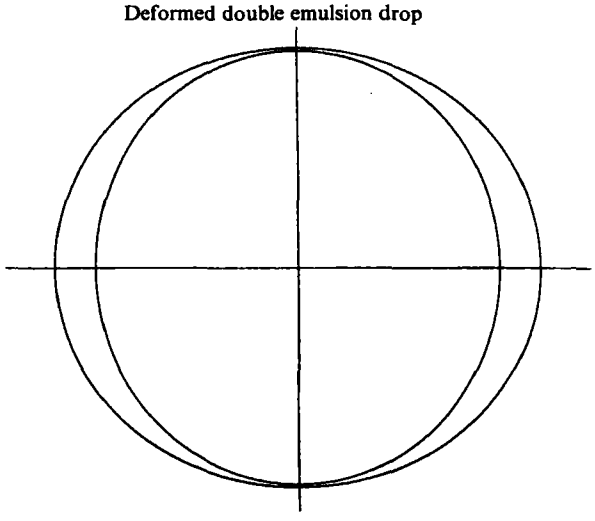

FIGURE 7. The deformed shape for system IA for $\epsilon = 0.88$ and $We^{(2)} = 0.1$ ($We^{(1)} = 0.1133$).

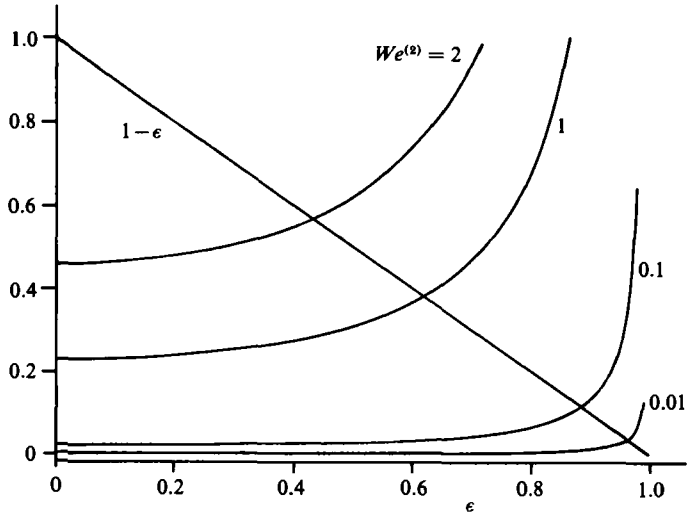

FIGURE 8. The point of rupture of the shell due to deformation caused by inertia as functions of ϵ with $We^{(2)}$ as parameter for system 1A. The curved lines represent the right-hand side of (4.25), and the critical thickness ϵ_c for rupture is the point of intersection with the function $1-\epsilon$ (i.e. the left-hand side of (4.25)). Only inside droplets smaller than ϵ_c could exist.

5. Sedimentation in a fluid at rest

In the previous two chapters we assumed the multiple drop to be held stationary by some external force $\tilde{f}$ in a moving fluid. In order to utilize these results for sedimentation ($\tilde{\Phi}^{(i)} = -\rho^{(i)} \boldsymbol{g} \cdot \boldsymbol{r}$, or $\tilde{a}^{(i)} = -\rho^{(i)} \boldsymbol{g}$) we have to require that the particle will reach a terminal velocity v_t ($= -V_\infty$). This being the case, the force balances (2.12) read

$$\hat{\boldsymbol{F}}^{(2)} - \hat{\boldsymbol{F}}^{(1)} + (\rho^{(1)} - \rho^{(2)}) V_0 \boldsymbol{g} = 0, \tag{5.1}$$

	$\rho^{(1)} < \rho^{(2)}$	$\rho^{(1)} > \rho^{(2)}$
$\rho^{(3)} < \rho^{(2)}$	$\rho^{(3)} < \rho^{(1)}$: 0 $\rho^{(3)} > \rho^{(1)}$: 0 or 2	1
$\rho^{(3)} > \rho^{(2)}$	1	$\rho^{(3)} < \rho^{(1)}$: 0 or 2 $\rho^{(3)} > \rho^{(1)}$: 0
$\rho^{(3)} = \rho^{(2)}$	$\epsilon^* = 1$ is a root; a second root $\epsilon^* < 1$ is possible if $6\eta^{(1)} < 4\eta^{(2)} - 3\eta^{(3)}$	

TABLE 2. The number of roots of (4.6)

with $V_0 = \frac{4}{3}\pi a^3$ the total volume of the drop.† Similarly

$$\hat{F}^{(1)} + (\rho^{(3)} - \rho^{(1)})\, V_i \boldsymbol{g} = 0, \quad V_i = \tfrac{4}{3}\pi(a\epsilon)^3. \tag{5.2}$$

Since both equations have to be satisfied simultaneously, it is clear that the physical parameters of the system (ϵ, a, $\rho^{(i)}$ and $\eta^{(i)}$) have to be related. Phrased differently, if the fluids involved are known (i.e. $\rho^{(i)}$ and $\eta^{(i)}$ are known) then only for very selected values of ϵ will (5.1) and (5.2) furnish the same terminal velocity v_t. To see this relation explicitly we first deduce from (5.1) and (5.2) an alternative relation

$$\hat{F}^{(2)} + [\rho^{(1)} V_m + \rho^{(3)} V_i - \rho^{(2)} V_0]\boldsymbol{g} = 0, \tag{5.3}$$

which is the force balance for the particle as a whole.

In order to satisfy (5.3) and (5.4) simultaneously the following must be true:

$$\frac{\hat{F}^{(2)}}{\hat{F}^{(1)}} = \frac{1}{\epsilon^3}\left[\frac{1-\rho_{21}}{\rho_{31}-1} + \epsilon^3\right]. \tag{5.4}$$

Recalling (4.16), it follows that the physical parameters are related by

$$\eta_{12}\left[\frac{1-\rho_{21}}{\rho_{31}-1} + \epsilon^3\right] = -\epsilon^2(1-\epsilon)\,\frac{6\eta_{13}\eta_{12} + \eta_{13}(2+3\eta_{32})\,(1-\epsilon)f + (1-\epsilon)^2 g_1}{2\eta_{13} + (1-\epsilon)\,h}. \tag{5.5}$$

Since the right-hand side of this equation is strictly non-positive, no ϵ, $0 \leqslant \epsilon < 1$, exists that will solve (5.5) unless $(1-\rho_{21})/(\rho_{31}-1) < 0$. As a matter of fact, the left-hand side of (4.6) increases monotonically from its $\epsilon = 0$ value of

$$\eta_{12}(1-\rho_{21})/(\rho_{31}-1),$$

with a horizontal slope towards $\eta_{12}(1-\rho_{23})/(1-\rho_{13})$ for $\epsilon \to 1$, which it reaches with the slope $3\eta_{12}$. On the other hand, the non-positive right-hand side of (4.6) has the following behaviour at these limits

$$\text{r.h.s.} \to \begin{cases} -2\epsilon^2\,\dfrac{(1+\eta_{13})\,(2+3\eta_{12})}{3+2\eta_{13}} & \text{as } \epsilon \to 0, \\ -3\eta_{12}(1-\epsilon) + O((1-\epsilon)^2) & \text{as } \epsilon \to 1. \end{cases} \tag{5.6}$$

This behaviour and a careful examination of figures 2 and 5 reveals the existence of one minimum of the right-hand side. Consequently we can write down the number of solutions of (5.5) as in table 2.

† Note that we have incompressible fluids, so that the volume remains unchanged no matter how the particle deforms.

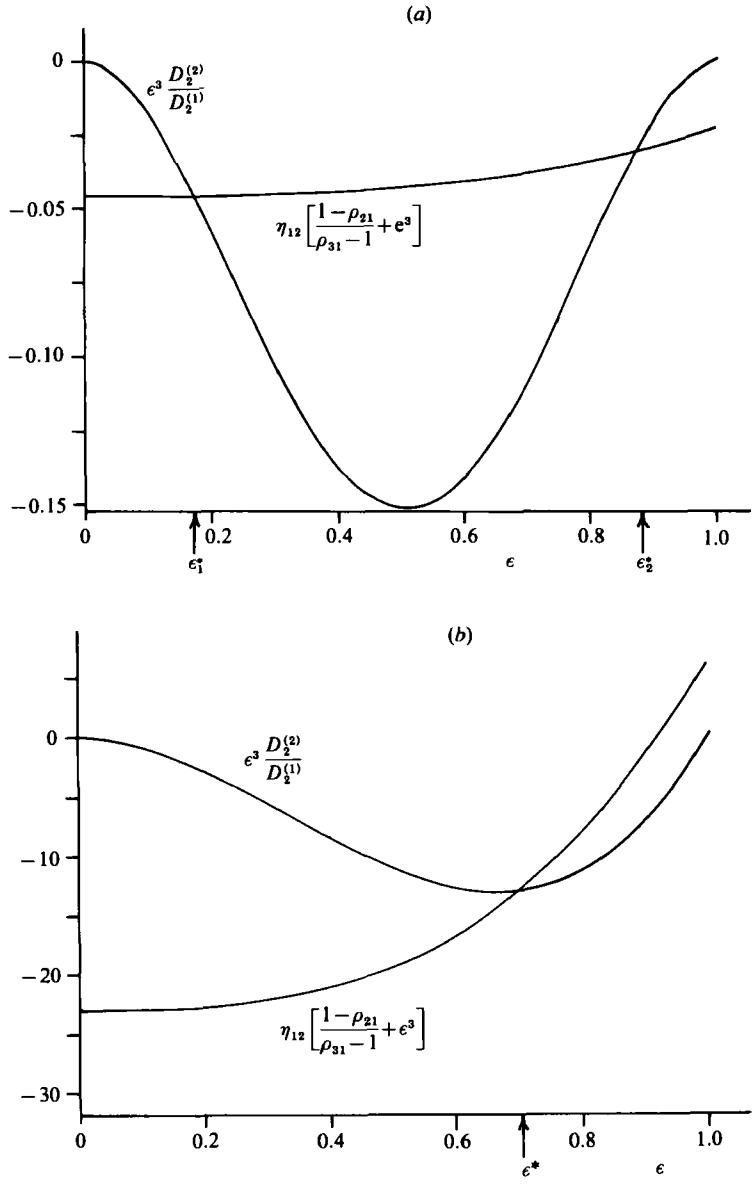

FIGURE 9 (a–c). For caption see facing page.

According to this table, (5.5) may have more than one root – termed ϵ^*. Testing all systems of table 1 we found only one system that has multiple roots: system 2 (see figure 9a). Yet, as pointed out in §4, this is one system for which the multiple drop is actually of type B. Since system 3 also seems to be of type B (Halwachs, Flashel & Schungel 1980) but has only one root, no conclusion with respect to the number of roots of (5.5) and the type of multiple drop (A, B or C) can be reached.

For all other systems only one root was found (see table 1: ϵ^*). This indicates that the size ratio of the inside to the shell region should be unique, i.e. that symmetric type-A droplets should be geometrically identical for a given system.

Before discussing our prediction of ϵ^* for the systems listed in table 1, it is worth

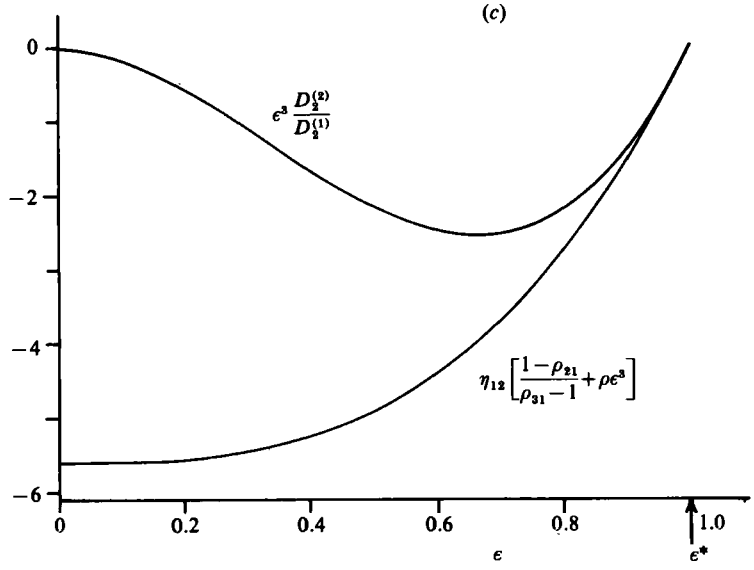

FIGURE 9. The size ϵ^* of the inside droplet as determined by a force balance for sedimentation. The cutpoint(s) furnish the admissible root ϵ^*. (*a*) System 2; (*b*) system 1C; (*c*) system 4.

while to point out a few general features. First, if the inside and continuous fluid densities match ($\rho^{(3)} = \rho^{(2)}$) then $\epsilon^* = 1$ is always a solution. As indicated in table 2, this will be the only solution if the double emulsion is of the W/O/W type, while for an O/W/O double emulsions a second root $\epsilon^* < 1$ may have to be reckoned with. Secondly, if we introduce the mean multiple drop density $\rho^{(m)}$ by

$$\rho^{(m)} V_0 = \rho^{(3)} V_i + \rho^{(1)} V_m, \tag{5.7}$$

then (up to the term η_{12}) the left-hand side of (5.5) can be related to $\rho^{(m)}$ by

$$\frac{1-\rho_{21}}{\rho_{31}-1}+\epsilon^3 = \frac{\rho^{(m)}-\rho^{(2)}}{\rho^{(3)}-\rho^{(1)}}. \tag{5.8}$$

In order for (5.5) to have a solution the right-hand side of (5.8) has to be negative. This then implies that the density difference $\rho^{(3)}-\rho^{(1)}$ dictates the sign of the terminal velocity v_t. If $\rho^{(3)} > \rho^{(1)}$ the particle will rise, while for $\rho^{(3)} < \rho^{(1)}$ the particle will settle. While this feature was to be expected on the basis of the different signs of the drag coefficients $D_2^{(2)}$ and $D_2^{(1)}$, it is in contradiction to all experiments in which the multiple droplet is generated by the rise of one droplet through a layer of heavy fluid ($\rho^{(3)} < \rho^{(1)}$) underlying a lighter fluid ($\rho^{(3)} < \rho^{(2)} < \rho^{(1)}$). Whether or not it suffices in these cases to study type-A drops with the inside droplet displaced from the centre or whether an only partially encapsulated 'inside' drop is called for has to await further study.†

It is interesting to see that for all systems studied (5.5) has a solution. This implies that with an inside drop radius of ϵ^* a perfectly symmetric type-A drop arrangement is possible in sedimentation. Whether or not such an arrangement is an absolutely stable one (or whether experimental systems adjust the shell thickness to satisfy the

† Note that Mercier *et al.* (1974) speak of an encapsulating layer of variable thickness. Li & Asher (1973) specifically mention complete encapsulation of the rising oxygen bubble.

constraint of a perfectly symmetric configuration) is another matter, which will require further study. We already know that our prediction for systems 5 and 6 cannot be used for the experiments, which were performed using a diffusion column. Only if these multiple drops could be produced by different means, such that low Reynolds numbers would be involved, would there be any basis for comparison.

In contrast with these rather large-Reynolds-number cases are the multiple droplets generated by means of a double emulsification. Figure 9(*b*) shows our sedimentation result for system 1C (no experimental data for ϵ^* have been reported for any of the systems of group 1), while figure 9(*c*) is based on the data of system 4. The graphs for system 3 are similar to figure 9(*b*), with $\epsilon^* = 0.84$ as root of (5.5). Since system 3 forms type-B multiple droplets, this result should be read as meaning 59.3 % of the drop to consist of liquid 3. What makes this system interesting for our situation is the sensitivity of ϵ^* to the values of the densities $\rho^{(3)}$ and $\rho^{(2)}$. Since no data have been provided, we estimated (in g/cm^3) $\rho^{(2)}$ to be 0.988 and $\rho^{(3)}$ as 1.00. Changing these values to 1.00 and 1.01 respectively decreases ϵ^* from 0.84 to 0.66. On the other hand, using the values 0.998 and 0.998 respectively furnishes $\epsilon^* = 1$. As mentioned before, $\epsilon^* = 1$ is always a (double) root of (5.5) for $\rho^{(2)} = \rho^{(3)}$ (see figure 9*c*). On the basis of this extreme sensitivity of ϵ^* to the actual values for $\rho^{(2)}$ and $\rho^{(3)}$, the discrepancy between our prediction $\epsilon^* = 1$ for system 4 and the experimental result $\epsilon^* = 0.338$ may partly be based on our assumption of $\rho_{32} = 1$.† Based on the extreme sensitivity of our results to the actual data, we expect rather dramatic changes if surfactants are accounted for (either a la Frumkin–Levich or by means of a stagnant cap). Experimentally the fundamental role of surfactants is well established: Starting from the very same single emulsion and merely changing the surfactants in the second emulsification step, one obtains – depending upon the type of surfactants used – either (perfectly symmetric) type-A -B or -C multiple drops (Florence & Whitehill 1981). In addition, these latter authors used a rather concentrated double emulsion. This contrasts with our individual type-A droplet study, which would be relevant only in a highly dilute double emulsion. If we assume that part of the abovementioned discrepancy is due to this difference in particle concentration, then the conclusion to be reached is that the thickness of the liquid shell should increase with increasing particle concentration. Since the resistance to mass transfer increases with increasing membrane thickness (e.g. Halwachs *et al.* 1980), the increase in permeation due to an increase in particle concentration (and consequently in surface area for the mass transfer) would at least partly be offset by such an increase in membrane thickness.

6. Summary and conclusion

In this paper we have studied the hydrodynamic behaviour of a type-A double emulsion droplet in the low-Reynolds-number region. For droplets generated in a diffusion column, differences from single-droplet behaviour do not seem to show up until the droplets are sufficiently large (Mercier *et al.* 1974; Mori *et al.* 1977). This implies that not all of the three Reynolds numbers involved are small. Thus such multiple drops are outside the scope of our low-Reynolds-number analysis. As a matter of fact, our inertial results show that such drops cannot exist in a perfectly concentric (and symmetric) configuration (recall (4.25) and the remarks following it). In addition, our sedimentation result, that perfectly concentric type-A drops will rise

† All of our results for system 4 are estimates, since no data have been provided.

for $\rho^{(3)} > \rho^{(1)}$ and settle for $\rho^{(3)} > \rho^{(1)}$, would not even allow the possibility of experimentally obtaining such droplets. They cannot be treated by our analysis, and it seems more appropriate to use medium-Reynolds-number calculations for shell regions of variable thickness. A zero-Reynolds-number analysis for spherical-cap regions has been attempted (Johnson & Sadhal 1983).

As far as multiple droplets, obtained by double emulsifications, are concerned we are in better shape, because of the low Reynolds numbers of those experiments. We do predict large particle size to be a source of particle breakdown, which seems to be in agreement with the experiments (Li 1981). On the basis of a force balance for sedimentation, we predict for type-A drops a unique size ratio for inside to total volume. Attempts to compare this result quantitatively with experiments encountered difficulties, since only for one single system has this ratio been listed. Unfortunately no other data had been provided. Estimating the data needed did not produce the expected agreement. Reasons for that discrepancy – other than the sensitivity of our result to the accuracy of data – have been advanced.

It is hoped that future detailed measurements will enable us to make quantitative comparisons. We are just at the beginning of the road, and problems like the role of surfactants or the stability of a type-A droplet – with respect to small displacements from the centre – need to be investigated carefully.

Appendix A. The Stokes solution coefficients

Let us define the following positive and finite-valued functions of ϵ:

$$h_1 = \frac{1-\epsilon}{1-\epsilon^5} = \frac{1}{1+\epsilon+\epsilon^2+\epsilon^3+\epsilon^4}, \tag{A 1}$$

$$g_1 = (4+7\epsilon+4\epsilon^2)\,h_1, \tag{A 2}$$

$$f = (1+\epsilon)(2+\epsilon+2\epsilon^2)\,h_1, \tag{A 3}$$

$$h_2 = (1+2\epsilon)\,h_1, \tag{A 4}$$

$$h_3 = (2+\epsilon)\,h_1, \tag{A 5}$$

$$h_4 = (2+4\epsilon+6\epsilon^2+3\epsilon^3)\,h_1, \tag{A 6}$$

$$h = (3+6\epsilon+4\epsilon^2+2\epsilon^3)\,h_1, \tag{A 7}$$

$$h_5 = (1+3\epsilon+\epsilon^2)\,h_1. \tag{A 8}$$

Then, with

$$K = 4\eta_{12}\eta_{13} + 2(1-\epsilon)f\eta_{13}(1+\eta_{32}) + (1-\epsilon)^2 g_1, \tag{A 9}$$

the coefficients are

$$D_2^{(2)} = 1 - B_2^{(2)} = \frac{3}{2} - \frac{1-\epsilon}{K}\,d_2^{(2)} = \frac{3}{2} - \frac{1-\epsilon}{K}\,(\eta_{13}f + \tfrac{1}{2}(1-\epsilon)\,g_1), \tag{A 10}$$

$$A_2^{(1)} = \frac{1}{K(1-\epsilon)}\,[2\eta_{13} + (1-\epsilon)\,h_4] = \frac{1}{K(1-\epsilon)}\,a_2^{(1)}, \tag{A 11}$$

$$B_2^{(1)} = \frac{\epsilon^3}{K(1-\epsilon)}\,[2\eta_{13}\epsilon^2 h_1 + (1-\epsilon)\,h_2] = \frac{\epsilon^3}{K(1-\epsilon)}\,b_2^{(1)}, \tag{A 12}$$

$$C_2^{(1)} = -\frac{1}{K(1-\epsilon)}\,[2\eta_{13}\,h_1 + (1-\epsilon)\,h_3] = -\frac{1}{K(1-\epsilon)}\,c_2^{(1)}, \tag{A 13}$$

$$D_2^{(1)} = -\frac{\epsilon}{K(1-\epsilon)}[2\eta_{13}+(1-\epsilon)h] = -\frac{\epsilon}{(1-\epsilon)K}d_2^{(1)}, \tag{A 14}$$

$$C_2^{(3)} = -\frac{1}{\epsilon^2}A_2^{(3)} = \frac{(1-\epsilon)}{K\epsilon^2}\eta_{13}h_5 = \frac{1-\epsilon}{\epsilon^2 K}c_2^{(3)}. \tag{A 15}$$

Appendix B. Explicit expression for the deformations

Equation (3.18) involves the functions $I_1^{(i)}$ and $H^{(i)}$. Applying all of the eight boundary conditions allows us after a considerable amount of manipulations to determine the deformations (3.20). With the definition

$$\gamma^{(i)}(r) = B_2^{(i)}[3C_2^{(i)}r^{-1}+A_2^{(i)}r^{-3}+\tfrac{1}{4}B_2^{(i)}r^{-6}]+C_2^{(i)}[A_2^{(i)}r^2+\tfrac{2}{3}C_2^{(i)}r^4] \tag{B 1}$$

it may then be shown that

$$\beta^{(2)}(1)-\rho_{12}\beta^{(1)}(1) = \gamma^{(2)}(1)-\rho_{12}\gamma^{(1)}(1)+\epsilon_{21}, \tag{B 2}$$

$$\beta^{(1)}(\epsilon)-\rho_{31}\beta^{(3)}(\epsilon) = \gamma^{(1)}(\epsilon)-\rho_{31}\gamma^{(3)}(\epsilon)+\epsilon_{13}. \tag{B 3}$$

In order to write down the functions ϵ_{ij} in a somewhat-condensed form it proves convenient to introduce the functions

$$f_1 = 4+16\epsilon+40\epsilon^2+55\epsilon^3+40\epsilon^4+16\epsilon^5+4\epsilon^6, \tag{B 4a}$$

$$f_2 = 2+4\epsilon+8\epsilon^2+7\epsilon^3+8\epsilon^4+4\epsilon^5+2\epsilon^6, \tag{B 4b}$$

$$F = \frac{1}{3}\left[(1-\epsilon)^2 f_1+2(1-\epsilon^2)(\eta_{12}+\eta_{13})f_2+4\frac{(1-\epsilon^3)(1-\epsilon^7)}{(1-\epsilon)^2}\eta_{12}\eta_{13}\right]. \tag{B 5}$$

Then, with

$$B_{15} = (7-\tfrac{40}{3}\epsilon^2)+\tfrac{16}{3}\epsilon^2\eta_{13}, \tag{B 6a}$$

$$B_{14} = \tfrac{16}{3}(1+\eta_{13}), \tag{B 6b}$$

$$B_{25} = -6+10\epsilon^2+\tfrac{4}{3}\epsilon^5-\tfrac{4}{3}\epsilon^2(3+\epsilon^3)\eta_{13}, \tag{B 7a}$$

$$B_{24} = -4+\tfrac{11}{3}\epsilon^3-6\epsilon^5-\tfrac{4}{3}(3+\epsilon^3)\eta_{13}, \tag{B 7b}$$

$$y_1 = -(1-\epsilon)(\tfrac{2}{3}+\tfrac{4}{3}\epsilon+2\epsilon^2+\epsilon^3)-\tfrac{2}{3}\eta_{13}(1+\epsilon+\epsilon^2), \tag{B 8a}$$

$$y_2 = 2[(1-\epsilon^5)+\eta_{13}+\epsilon^5\eta_{12}] \tag{B 8b}$$

$$y_3 = -(1-\epsilon)(1+2\epsilon+\tfrac{4}{3}\epsilon^2+\tfrac{2}{3}\epsilon^3)-\tfrac{2}{3}\eta_{13}(1+\epsilon+\epsilon^2), \tag{B 8c}$$

$$y_4 = 5(1-\epsilon^2)+2(\eta_{12}+\eta_{13}\epsilon^2), \tag{B 8d}$$

i.e.

$$y_2 y_3 - y_1 y_4 = (1-\epsilon)F, \tag{B 9}$$

we introduce

$$z_{i3} = \frac{1}{F}[y_2 B_{i5}-y_4 B_{i4}], \tag{B 10}$$

$$\nu_{21} z_{i4} = \frac{1}{F}[y_3 B_{i4}-y_1 B_{i5}], \quad \nu_{21} = \eta_{21}\rho_{12}. \tag{B 11}$$

Letting now

$$C_1 = -\frac{1}{30K^2}\{a_2^{(1)}[\eta_{13}(1+\epsilon+\epsilon^2)+\tfrac{5}{2}(1-\epsilon)(2+\epsilon)]$$
$$+b_2^{(1)}[2\eta_{13}(1+\epsilon+\epsilon^2)+\tfrac{5}{2}(1-\epsilon)(1+2\epsilon+3\epsilon^2)]$$
$$-\epsilon c_2^{(1)}[2\eta_{13}\epsilon(1+\epsilon+\epsilon^2)+\tfrac{5}{2}(1-\epsilon)(3+2\epsilon+\epsilon^2)]$$
$$-d_2^{(1)}[\eta_{13}(1+\epsilon+\epsilon^2)+\tfrac{5}{2}(1-\epsilon)(1+2\epsilon)]\}, \tag{B 12}$$

$$C_2 = \frac{1}{20K^2}\{a_2^{(1)}[10(1-\epsilon)+2(\eta_{13}+\epsilon\eta_{12})]$$
$$+b_2^{(1)}[5(1-\epsilon^4)+4(\eta_{13}+\epsilon^4\eta_{12})]$$
$$-\epsilon c_2^{(1)}[20(1-\epsilon)+4(\epsilon\eta_{13}+\eta_{12})]$$
$$-d_2^{(1)}[5(1-\epsilon^2)+2(\eta_{13}+\epsilon^2\eta_{12})], \tag{B 13}$$

we have

$$\epsilon_{21} = D_2^{(2)}\chi_{21} + \frac{\rho_{12}d_2^{(1)}}{(1-\epsilon)^2}\left\{\frac{z_{13}C_1+\nu_{21}z_{14}C_2}{1-\epsilon} - \mathscr{D}_1\right\}, \tag{B 14a}$$

$$\epsilon_{13} = \frac{D_2^{(2)}}{\epsilon^3(1-\epsilon)}\chi_{13} + \frac{d_2^{(1)}}{\epsilon^3(1-\epsilon)^2}\left\{\frac{z_{23}C_1+\nu_{21}z_{24}C_2}{1-\epsilon} - \mathscr{D}_2\right\}. \tag{B 14b}$$

Here we have introduced the functions

$$\chi_{21} = -\frac{19}{20}+\frac{7}{30}\frac{1-\epsilon}{K}d_2^{(2)} + \frac{1}{10}\frac{\rho_{12}z_{14}}{1-\epsilon}\left(2+\frac{1-\epsilon}{K}d_2^{(2)}\right), \tag{B 15a}$$

$$\chi_{13} = \frac{z_{24}}{10}\left(2+\frac{1-\epsilon}{K}d_2^{(2)}\right), \tag{B 15b}$$

$$\mathscr{D}_1 = \frac{1}{K^2}\{a_2^{(1)}[\tfrac{4}{3}-\tfrac{7}{5}\epsilon+\tfrac{4}{15}\eta_{13}]+b_2^{(1)}[\tfrac{2}{3}-\tfrac{4}{5}\epsilon^4+\tfrac{8}{15}\eta_{13}]$$
$$-\epsilon c_2^{(1)}[\tfrac{13}{15}-\tfrac{8}{3}\epsilon+\tfrac{8}{15}\eta_{13}\epsilon]-d_2^{(1)}[\tfrac{2}{3}-\tfrac{17}{30}\epsilon^2+\tfrac{4}{15}\eta_{13}], \tag{B 16a}$$

$$\mathscr{D}_2 = \frac{1}{K^2}\{a_2^{(1)}[-1+\tfrac{3}{2}\epsilon-\tfrac{29}{60}\epsilon^3-\tfrac{1}{15}\eta_{13}(3+\epsilon^3)]+b_2^{(1)}[-\tfrac{1}{2}+\tfrac{61}{30}\epsilon^3$$
$$-\tfrac{3}{2}\epsilon^4-\tfrac{2}{15}\eta_{13}(3+\epsilon^3)]-\epsilon c_2^{(1)}[-\tfrac{3}{2}+2\epsilon+\tfrac{6}{5}\epsilon^4-\tfrac{2}{15}\eta_{13}\epsilon(3+\epsilon^3)]$$
$$-d_2^{(1)}[-\tfrac{1}{2}+\tfrac{3}{2}\epsilon^2-\tfrac{23}{20}\epsilon^3-\tfrac{1}{15}\eta_{13}(3+\epsilon^3)]\}. \tag{B 16b}$$

REFERENCES

Aris, R. 1962 *Vectors, Tensors and the Basic Equations of Fluid Mechanics*, chap. 10. Prentice-Hall.

Brodin, A. F., Kavaliunas, D. R. & Frank, S. G. 1978 Prolonged drug release from multiple emulsions. *Acta Pharma. Suec.* **15**, 1–12.

Clift, R., Grace, J. R. & Weber, M. E. 1978 *Bubbles, Drops and Particles*. Academic.

Florence, A. T. & Whitehill, D. 1981 Some features of breakdown in water-in-oil-in-water multiple emulsions. *J. Coll. Interface Sci.* **79**, 243–256.

Halwachs, W., Flashel, E. & Schungel, K. 1980 Liquid membrane transport – a highly selective separation process for organic solutions. *J. Membrane Sci.* **6**, 33–34.

Happel, J. & Brenner, H. 1973 *Low Reynolds Number Hydrodynamics*, §4.23. Noordhoff.

JOHNSON, R. E. & SADHAL, S. S. 1983 Stokes flow past bubbles and drops partially coated with a thin films. Part 2. Thin films with internal circulation – a perturbation solution. *J. Fluid Mech.* **132**, 295–318.

LAMB, H. 1932 *Hydrodynamics*, 6th edn, chap. 11. Cambridge University Press.

LI, N. N. 1971 Separation of hydrocarbons by liquid membrane permeation. *Ind. Engng Chem. Process Des. Dev.* **10**, 215–221.

LI, N. N. & ASHER, W. J. 1973 Blood oxygenation by liquid membrane permeation. *Chem. Engng in Medicine, Adv. Chem. Ser.* **118**, 1–14.

LI, N. N. & SHRIER, A. L. 1972 Recent developments in separation science, vol. I, p. 163. Chemical Rubber Co.

MARTIN, T. P. & DAVIES, G. A. 1976 The extraction of copper from dilute aqueous solutions using a liquid membrane process. *Hydrometall.* **2**, 315–334.

MERCIER, J. L., DA CUNHA, F. M., TEIXEIRA, J. C. & SCOFIELD, M. P. 1974 Influence of enveloping water layer on the rise of air bubbles in Newtonian fluids. *Trans. ASME* E: *J. Appl. Mech.* **96**, 29–34.

MORI, Y. M., KOMOTORI, K., HIGETA, K. & INADA, J. 1977 Rising behavior of air bubbles in superposed liquid layers. *Can. J. Chem. Engng.* **55**, 9–12.

RUSHTON, R. & DAVIS, G. A. 1983 Settling of encapsulated drops at low Reynolds numbers. *Intl J. Multiphase Flow* **9**, 337–342.

SELECKI, A. & GRADON, L. 1972 Über den Verdampfungsmechanismus eines sich in einer nicht mischbaren Flüssigkeit bewegenden Flüssigkeitstroptens. *Chem. Ing. Tech.* **44**, 1077–1081.

SIDEMAN, S. & TAITEL, Y. 1964 Direct contact heat transfer with change of phase: evaporation of drops in an immiscible liquid medium. *Intl J. Heat Mass Transfer* **7**, 1273–1279.

TAYLOR, J. D. & ACRIVOS, A. 1964 On the deformation and drag of a falling viscous drop at low Reynolds number. *J. Fluid Mech.* **18**, 466–476.

ULBRECHT, J. J., STROEVE, P. & PRABODH, P. 1982 Behavior of double emulsions in shear flows. *Rheol. Acta* **21**, 593–597.